Supporting information

for

Synthesis–Structure–Activity Relations in Fe-CHA for C–H Activation: Control of Al Distribution by Interzeolite Conversion

Julien Devos,† Max L. Bols,† Dieter Plessers,† Cédric Van Goethem ǂ, Jin Won Seo^, Son-Jong Hwang°, Bert F. Sels† and Michiel Dusselier†,*

Corresponding author: michiel.dusselier@kuleuven.be

† Center for Sustainable Catalysis and Engineering (CSCE), KU Leuven, Celestijnenlaan 200F, B-3001 Leuven, Belgium
ǂ Centre for Membrane Separations, Adsorption, Catalysis and Spectroscopy for Sustainable Solutions (cMACS), Celestijnenlaan 200F, B-3001 Leuven, Belgium
^ Department of Materials Engineering (MTM), KU Leuven, Kasteelpark Arenberg 44 – bus 2450, B-3001 Leuven, Belgium
° Division of Chemistry and Chemical Engineering, California Institute of Technology, Pasadena, California 91125, USA.

Table of Contents

Section S.1. Characterization of synthesized SSZ-13 zeolites.

Table S1 contains various characterization data from zeolite synthesis and information from Co^{II} exchange of SSZ-13 syntheses from different sources (IZC vs 'amorphous"). Table S2 demonstrates identical TGA behaviour over a selection of differently synthesized SSZ-13 samples (not only source variations). Figures S1-S4 provide extensive characterisation of zeolite synthesis demonstrated in Table S1, showing data from powder X-ray diffraction, nitrogen physisorption, TGA and SS NMR respectively.

Table S1. Synthesis and characterization of SSZ-13 (CHA) zeolites made with different T-atom sources.

Sampe name[a]	H_2O/Si	Si/Al_B [b]	Synthesis time	Synthesis Temp (°C)	Phase	Yield[c]	Si/Al_F[d]	DCC = Co/Al_F [d]	V_{micro} (cm^3/g)[e]
Am*-1	18	37	6 days	160	CHA	0.74	25	0.008	
Am*-2	18	39	6 days	160	CHA	0.84	30	0.004	
Am*-3	18	40	6 days	160	CHA	0.84	30	0.003	0.33
IZC-1	18	40	6 days	160	CHA	0.77	39	0.22	
IZC-2	18	40	6 days	160	CHA	0.78	36	0.25	0.31
IZC-3	18	40	6 days	160	CHA	0.77	36	0.24	

[a] All syntheses originate from synthesis batch compositions: ~**1**SiO_2:**40**Al^{-1}:**0.35**$TMAda^+$:**0.35**OH^-:**18**H_2O after 6 days at 160°C. 'Am*-x': using LUDOX HS-40 and Al(OH)3, 'IZC-x': using CBV780 (US-Y) as sources. [b] Si/Al_B= batch Si/Al ratio; [c] Yield = dry product weight (g)*(1-0.2 wt. fraction OSDA)) / initial $(SiO_2+AlO_2)_{dry}$ (g); [d] product zeolite Si/Al ratio from ICP-AES; [e] from t-plot in N_2-physisorption (adsorption branch)

Table S2. Summary of elemental (ICP-AES) and thermogravimetric analysis (TGA) for CHA zeolites.

Sample name[a]	**Si/Al_F[b]**	**Al/unit cell[b]**	**Al/cage [c]**	**$TMAda^+$/cage [d]**
Am*-3	30	1.2	0.39	1.11
IZC-St.1	31	1.1	0.38	0.95
IZC-2[e]	36	1.0	0.32	1.12
OH-1	45	0.8	0.26	1.03
OH-3	43	0.8	0.28	1.10
OH-13	40	0.9	0.29	1.06
Time-4	35	1.0	0.33	0.94
H_2O-12	31	1.1	0.38	1.07
Temp-2	29	1.2	0.40	1.20

[a]Sample names from Table S1 and Table S4.
[b]Determined by ICP-AES assuming 100% framework Al (from ^{27}Al MAS NMR, Figure S4). The unit cell contains 36 T-atoms.
[c]Determined by ICP-AES assuming 100% framework Al. Given one Al per net surrounding a cage (i.e. 36 T-atoms, Si/Al=35), its charge can be distributed among the three cornering *cha* cages. Hence counting in full T-atoms, a cage totals 12 full T-atoms, while the net of T-atoms needed to form the cage equals 36 T-atoms. Also see Fig. S5.
[d]Calculated from TGA results where on average 20wt% of organic is lost. The remaining weight is calculated to be pure SSZ-13 ($SiO_2+AlO_2^-$) consisting of 1 cage per 12 T-atoms (TO_2).
[e] TGA pattern shown in Figure S3.

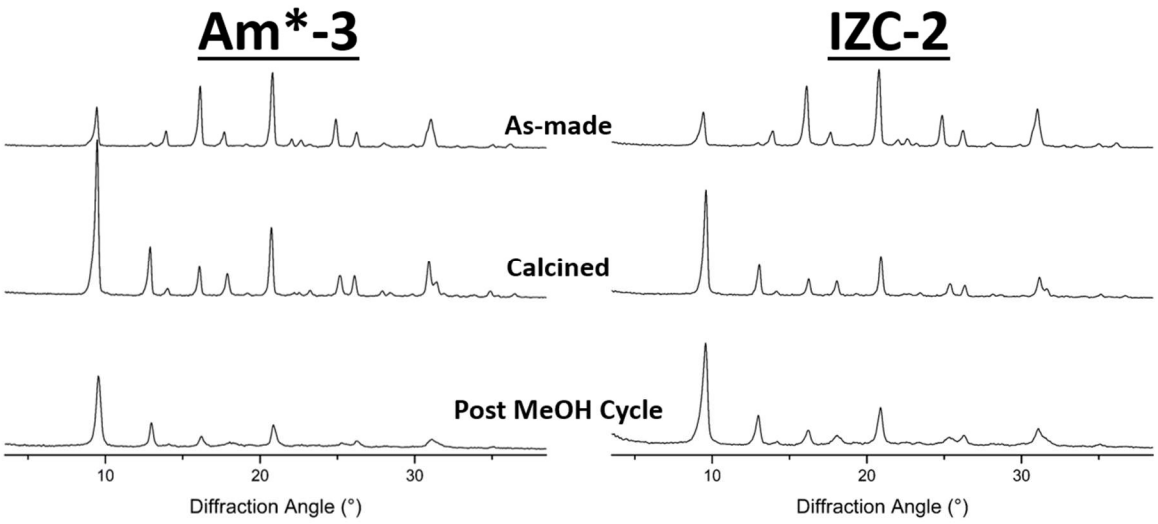

Figure S1. Powder XRD diffractograms (at various stages) of SSZ-13 made from amorphous sources (Am*-3, left) and by IZC (IZC-2, right). Each sample was measured for 10 minutes. The y-axis quantifies absolute counts.

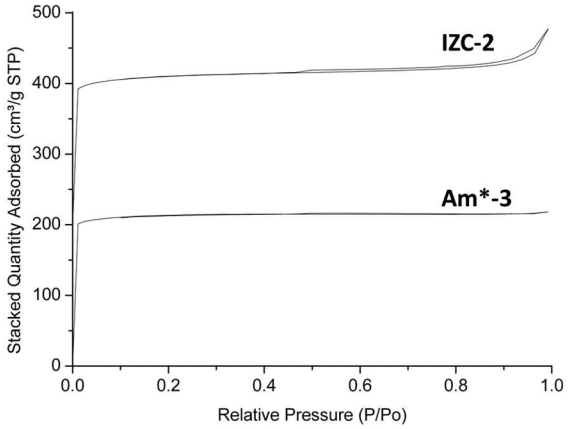

Figure S2. Representative nitrogen sorption isotherms of calcined high silica SSZ-13 materials made from amorphous sources (Am*-3) and by IZC (IZC-2). IZC-2 is shifted up by 200 cm^3/g in the stack.

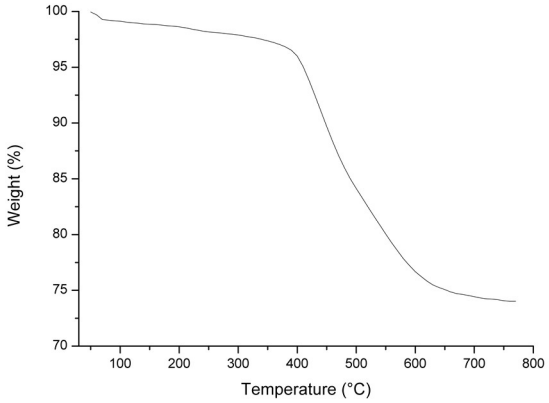

Figure S3. Typical thermogravimetric analysis (TGA) of as-synthesized high silica SSZ-13 (IZC-2).

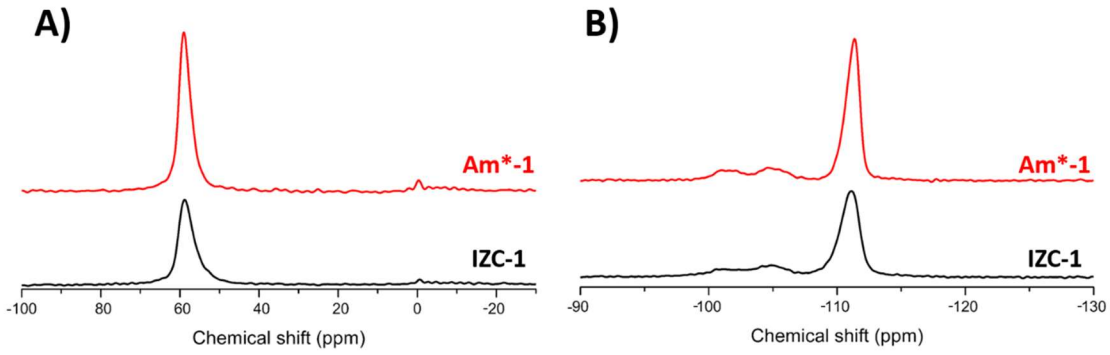

Figure S4. ^{27}Al SS NMR (A) and ^{29}Si SS NMR (B) of calcined high silica SSZ-13 materials made from amorphous sources (Am*-1) and by IZC (IZC-St.1).

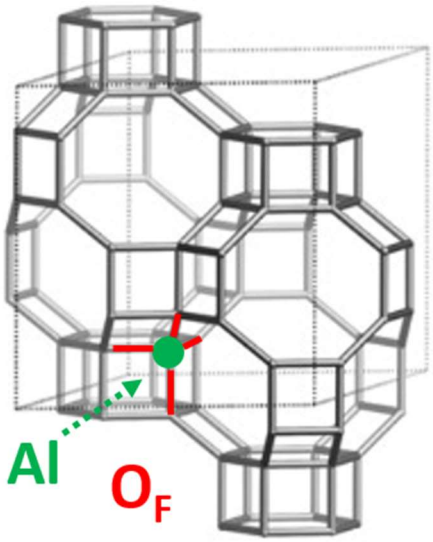

Figure S5. Illustration of Al T-atom (green dot) cornering three *cha*-cages and one double-six-membered ring (d6r). Charge compensation is possible on the adjacent framework O_F (red bar). Each of these O_F allows charge compensation from their adjacent voids, opening plenty of options for charge compensation even within this framework with only one crystallographically distinct T-site. Framework Si/Al_F=35 implicates one charge compensation per unit cell (36 T atoms, indicated with dotted lines) and also one charge per three *cha* cages. The charge can be compensated from within one of these adjacent cages. 12 fully counted T-atoms equal one cage. Physically, the net surrounding 1 cage is made up of 36 T-atoms (each counted 1/3 in each cage). A Si/Al ratio of 11:1 (total 12 T-atoms) thus offers one full charge per cage. For more information on such counts, see Dusselier and Davis, *Chem. Rev.* **2018** 118 11 5265-5329.

Section S.2. Quantification of divalent cation capacity (DCC) by Cobalt exchange.

The link between MeOH productivity and DCC validates the latter as an efficient tool to identify suitable synthesis recipes for TMI-hosting zeolites, as shown in the main text (Section 3.3). Nevertheless, DCC from Co-exchange does not automatically implicate quantification of Al pairs (2 Al in a 6MR), an optimal requirement for the proposed active site for MPO by Bols et al.[1] DR NIR-UV-Vis spectroscopy on a representative Co,Na-SSZ-13 sample (Time-3) assigns $Co^{2+}(H_2O)_6$ as the sole spectroscopic feature in the visual region (14.000 cm^{-1}-25.000 cm^{-1}). A major (right-tailed) peak at ±19.500 cm^{-1} can be observed (Figure S6), typical for a d-d electronic transition of isolated, octahedrally coordinated, hydrated Co^{2+}.[2] By keeping the exchange procedure constant, differences in sample loading are believed to be caused by the interactions of cobalt with Al-framework sites, rather than by exchange kinetics alone.[2] The standard DCC procedure using an aqueous 0.05 M $Co(NO_3)_2$ solution at room temperature indicates quasi-saturation after a number of consecutive Co^{2+} exchanges (150 cm^3 solution g^{-1}, ambient temperature, no pH adjustment), also for SSZ-13 with high uptake (Figure S7).
A TEM-EDX mapping (Figure S8) of Co-exchanged SSZ-13 with high DCC (Time-2) highlights the homogenous elemental distribution of Si, Al and also Co within individual crystals. Therefore, it can be assumed that all internal exchange sites can be reached. (Quasi)-saturation explains the reproducibility of DCC results with low variation, despite potential experimental variability in the many steps regarding synthesis, post-treatment, exchange and elemental analysis combined (Figure S7). For example, seven independent SSZ-13 resulting from identical standard synthesis recipes all have very similar DCC (Co/Al= 0.23(±0.01)). It was concluded that most variability within identical synthesis recipes can be attributed to tiny synthetic variations within the same recipe, most prominent in recipes close to the phase selectivity border of SSZ-13 (e.g. the large error bars at both low and high (TMadaOH)/Si concentrations, Figure 1A main manuscript). Given the kinetically controlled Al-distribution hypothesis, this is also not unexpected.

Co speciation in SSZ-13 was not evaluated under dehydration conditions in DR-UV-vis or FT-IR (as in the works of Dědeček et al). Co-Al moieties within zeolites show complex interactions during dehydration, including possible diffusion of dehydrated Co(II) into the double 6-ring (d6r).[3] Comparing Co loadings of different SSZ-13 samples after exchange at room temperatures allows discrimination between *isolated Al* and *proximate Al* arrangements. Mlekodaj et al. were the first to discriminate *proximate Al* arrangements in SSZ-13 – by spectroscopy at dehydration temperatures- into next-nearest-neighboring Al (AlSiAl), *paired Al* (AlSiSiAl, in a 6MR) and *close unpaired Al* sequences facing the same cavity.[3] The latter fraction cannot be neglected for SSZ-13, as Mlekodaj et al. demonstrated their high prevalence in Co-exchanged Na-SSZ-13, using similar exchange conditions as described in this work (experimental 2.1.2). *Close unpaired Al* arrangements are sequences of $AlSi_nAl$ (with n≥2) that can compensate $Co^{II}(H_2O)_6$ but unable to accommodate bare Co^{II} with dehydration. Discerning such arrangements within SSZ-13 was not in the scope of this work.

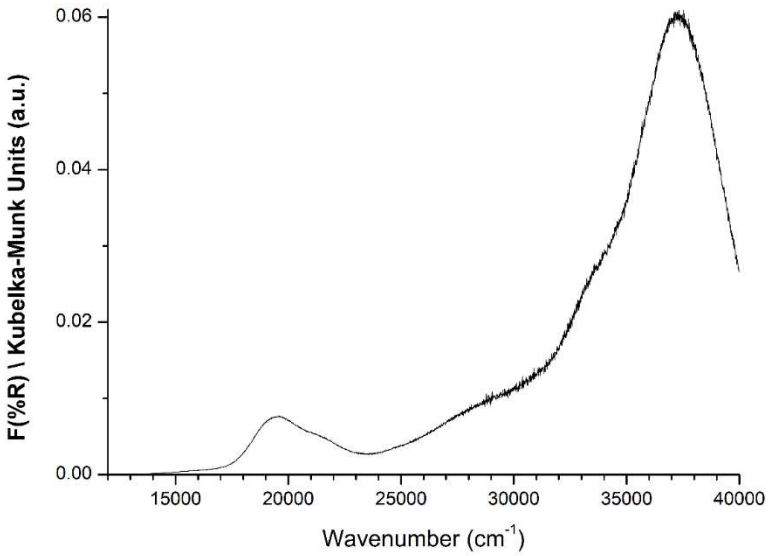

Figure S6. Diffuse reflectance UV−visible absorption spectrum of room temperature (wet) Co,Na-SSZ-13 with high Co/Al (Time-3, Table S4).

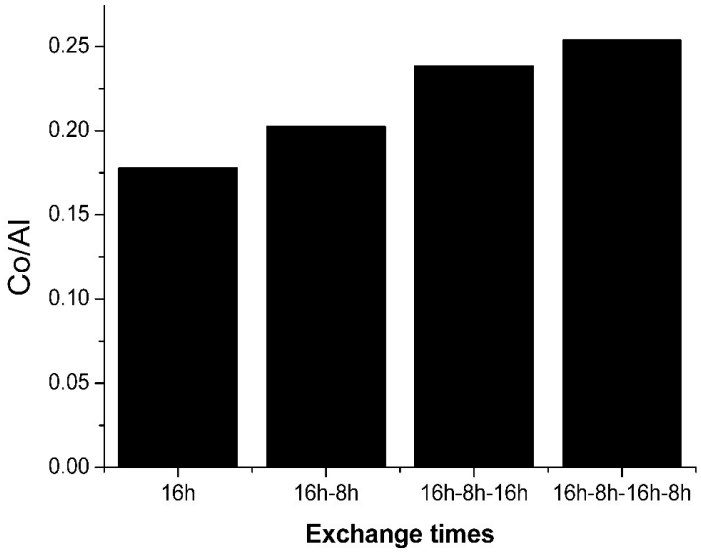

Figure S7. Co-uptake of SSZ-13 (IZC-St.3, Table S4) after multiple Co exchanges. Triple exchange (16h-8h-16h) Co/Al values are used as reference value for DCC.

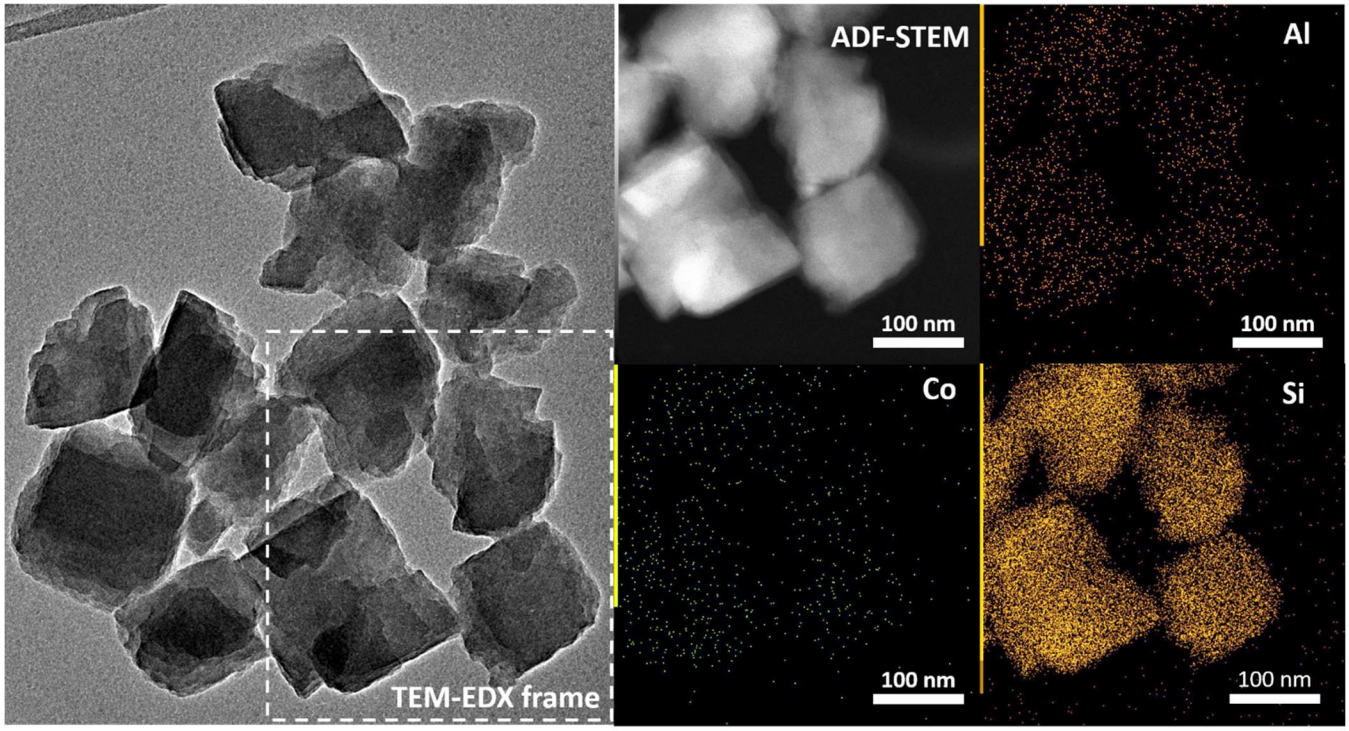

Figure S8. TEM image (left) of a representative Co-exchanged SSZ-13 with high DCC (Time-2). ADF-STEM image and elemental mapping (STEM-EDX) of Si, Al, and Co highlights the homogenous elemental distribution of these elements within the represented crystals. Zoom in for better resolution of Co and Al mapping.

Section S.3. Characterization of Fe-SSZ-13 materials for methane partial oxidation (MPO).

Figure S9-S10 demonstrates inhomogeneous Fe deposition on SSZ-13 zeolites from TEM imaging. In Section 3.1, DR NIR-UV–vis results confirm the presence of α-Fe species as defined by Bols et al. (Figure S11). Table S3 provides an overview of MPO properties of two materials tested for DR NIR-UV-VIS (Am*-1 and IZC-St.1).

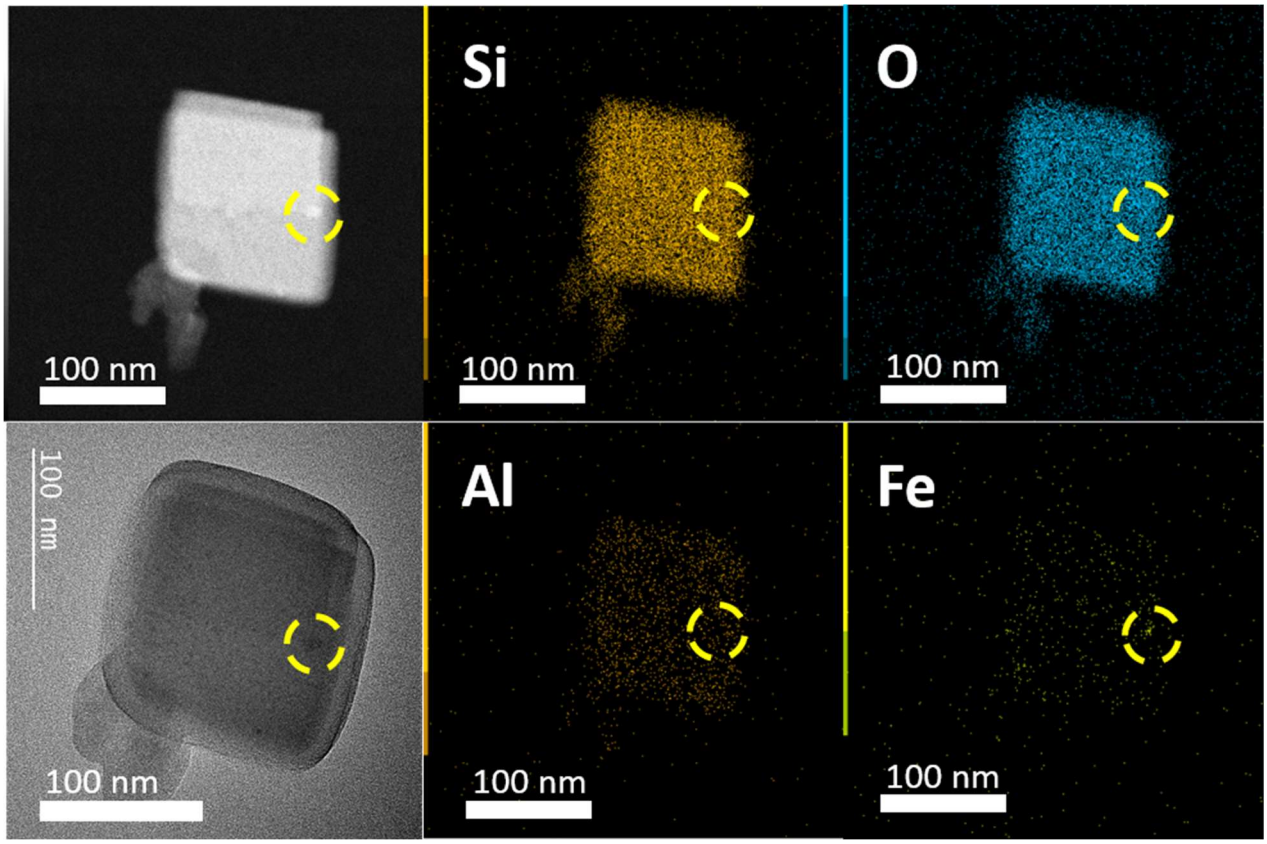

Figure S9. STEM-EDX mappings of Fe-exchanged SSZ-13, including elemental mapping for Si, O, Al and Fe (IZC-2; Si/Al=36; Fe/Al=0.17). Zoom in for a better resolution of the Al and Fe elemental mappings.

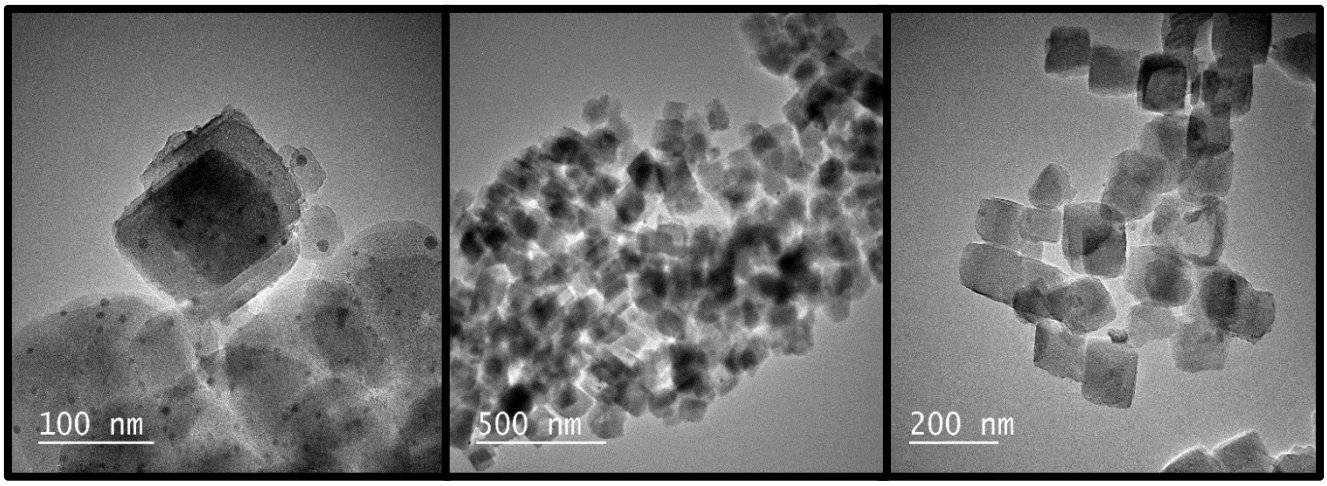

Figure S10. TEM images of Fe-exchanged SSZ-13, before methane partial oxidation (IZC-2; Si/Al=36, Fe/Al=0.17).

S.3.1. Further characterization of SSZ-13 zeolites synthesized from different sources.

DR NIR-UV–vis spectra of two SSZ-13 samples from different sources are recorded at each step of the reaction cycle. Sample 'IZC-St.1' is an identical synthesis by means of ingredients and procedures to the syntheses described in Table S1 (IZC-1), apart from a minute difference in the batch composition (Table S4, section S.4).

Diffuse reflectance spectroscopy (DRS- UV–vis–NIR*)*

In the UV–vis–NIR energy range diffuse reflectance was performed on a Varian Cary 5000 UV–vis–NIR spectrophotometer at room temperature against a halon white reflectance standard in the 4 000–40 000 cm^{-1} energy range. All treatments before in situ spectroscopic measurements were performed in the quartz U-tube/flow cell.

Preparation of Fe-exchanged zeolite for DR NIR-UV–vis tests. Zeolites used for DR-UV-vis-NIR are exchanged with $Fe(acac)_3$ and have slightly different exchange conditions than in Section 2.2.1. Samples Am*-1 and IZC-St.1 have exchange concentrations of 9.0 mM (27ml/g zeolite) and 9.7 mM (29ml/g zeolite) respectively.

Treatment procedure. The treatment procedure consists of an activation step in a 20 mL/min flow of He comprising a heating ramp of 10°C/min to the end temperature of 900°C which is maintained for 2 h (step 1), treatment in a 5% N_2O/He atmosphere for 20 min at 160 °C (step 2), and a 30 min treatment in 30 mL/min CH_4 flow at room temperature (step 3). Also see experimental Section 2.2 in main manuscript.

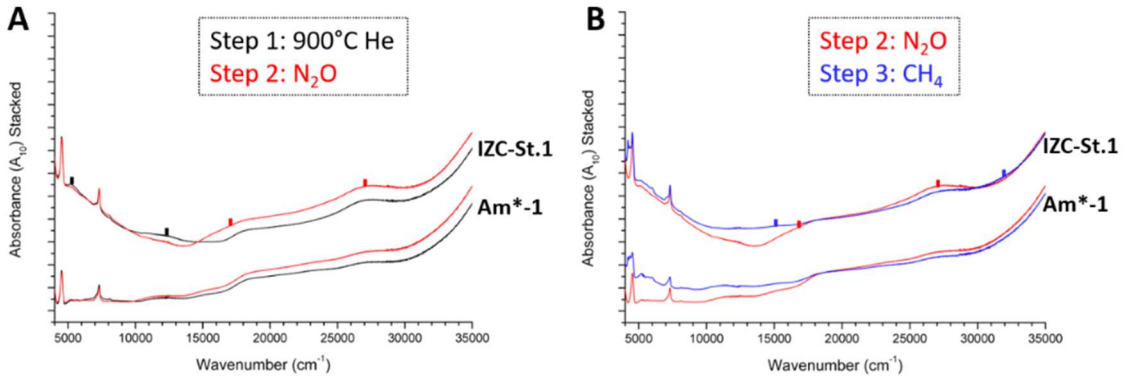

Figure S11. A) DR-UV–vis–NIR spectra of IZC-St.1 (top) and Am*-1 (bottom). (A) The black spectrum is measured after He treatment at 900 °C, the red spectrum is measured after subsequent reaction in N_2O atmosphere at 180 °C. (B) The red spectrum is the same as the red spectrum in A, and the blue spectrum is measured after subsequent reaction with CH_4 at room temperature.

DR-UV-vis-NIR spectra in figure S11 for sample IZC-St.1 exposes the presence of characteristic absorbance features typical for stepwise activation of Fe-SSZ-13 reaction centers:[1] features at 5 400 and 13 000 cm^{-1} representing α-Fe after He treatment at 900°C (step 1, features indicated in black), features at 17 500 and 27 000 cm^{-1} representing α-O after N_2O treatment (step 2, features indicated in red) and features at 15 000 and 32 000 cm^{-1} indicating interaction of the newly transformed Fe site with methane. In contrast, the Am*-1 sample show no large changes in the UV-VIS region, suggesting the present Fe species are largely unreactive. For both samples change is observed at 4210 and 4315 cm^{-1}, attributed to combination bands of methane, indicating that methane was effectively introduced in the SSZ-13 zeolites. In accordance to the detailed spectroscopic study of Bols et al.,[1] it is concluded that CH_4 reacts indeed over the Fe centers to form MeOH. with very different efficiency on both materials.

These 2 samples, IZC-St.1 and Am*1 again confirm the same DCC and MeOH productivity differences (Table S3) as the ones presented in Table 1. IZC-St.1 produces 21.7 µmol per gram SSZ-13 at an efficiency of MeOH/Fe= 0.38, while Am*-1 only yielded ~0.3 µmol per gram SSZ-13 (MeOH/Fe=0.01). It is worth noting that, again, the DCC trend tends to reflect the MeOH productivity much better than Fe/Al (Fe content), as reported in Figure 3 in the main text. The samples in Table 1 thus behave very similar to those in Table S3.

Table S3. DCC of SSZ-13 used for zeolites made with different T-atom sources.[a]

Exchange form	*Amorphous sources (Am*-1)*	*US-Y (Si/Al=40) source (IZC-St.-1)*
Fe.H-SSZ-13	Fe/Al = 0.05 (0.17 wt%) MeOH = 0.3 µmol/g[b] MeOH/Fe= 0.01	Fe/Al = 0.12 (0.32 wt%) MeOH = 21.7 µmol/g MeOH/Fe = 0.38
Co. Na-SSZ-13	Co/Al = 0.01	Co/Al = 0.24

[a] The compared samples are made according to identical synthesis, exchange and activation procedures.[b] MeOH quantification close to detection limits.

Section S.4. DCC variation in SSZ-13 made from interzeolite conversion (IZC)

Table S4 contains data of zeolite synthesis and information from Co^{II} exchange of IZC based SSZ-13 materials. Each single parameter variation is separated in series (Series I-IV). The DCC results are highlighted in Figure 1-2. Figure S12 and S13 represents additional characterisation data, as measured for some of the representative samples of different synthesis series. Section S4.1. concerns a deconvolution of synthesis parameter effects on DCC, while Section 4.2. concerns the effects of increasing solid yields on DCC.

Table S4.: Synthesis and characterization of SSZ-13 (CHA) zeolites made from IZC under different conditions.

Sample name[a]	H_2O/Si	OSDA-OH^-/Si	Synthesis Temp (°C)	Synth. time	Formed phase	Yield[b]	Si/Al_F[c]	Co^{2+}/Al_F [c] DCC	V_{micro} (cm^3/g)
I) Standard samples: **1**SiO2:**40**Al^{-1}:**0.35** $TMada^+$:**0.35**OH^-:**12.5** H_2O with CBV780 as starting material									
IZC-St.1	12.5	0.35	160	4 days	CHA	0.71	31	0.24	0.33
IZC-St.2	12.5	0.35	160	4 days	CHA	0.75	39	0.24	0.31
IZC-St.3	12.5	0.35	160	4 days	CHA	0.74	39	0.23	0.31
IZC-St.4	12.5	0.35	160	4 days	CHA	0.69	31	0.21	0.29
IZC-St.5	12.6	0.35	160	4 days	CHA	0.63	34	0.24	/
IZC-St.6	12.4	0.35	160	4 days	CHA	0.79	40	0.24	/
IZC-St.7	12.5	0.35	160	4 days	CHA	0.79	37	0.21	0.31
<IZC-St.>[d]	12.5	0.35	160	4 days	CHA	0.73(±0.06)	36 (±4)	0.23(±0.01)	0.31 (±0.01)
II) OH-series: Variation of OSDA-OH concentration : [$TMAda^+$-OH^-]/Si: [0.10-0.67] (no other OH source present so $TMAda^+$-OH = OH^-).									
OH-1	12.5	0.10	160	4 days	CHA+	0.84	45	0.01	/
OH-2	12.7	0.10	160	4 days	CHA	0.75	48	0.07	/
OH-3	12.5	0.15	160	4 days	CHA	0.9	43	0.11	0.31
OH-4	12.4	0.15	160	4 days	CHA	0.87	47	0.07	/
OH-5	12.6	0.17	160	4 days	CHA	0.88	38	0.11	/
OH-6	12.5	0.20	160	4 days	CHA	0.85	45	0.08	/
OH-7	12.5	0.25	160	4 days	CHA	0.82	43	0.15	0.29
OH-8	12.5	0.25	160	4 days	CHA	0.77	48	0.22	/
OH-9	12.6	0.30	160	4 days	CHA	0.77	40	0.18	0.29
OH-10	12.5	0.30	160	4 days	CHA	0.67	41	0.25	/
<IZC-St.>[d]	12.5	0.35	160	4 days	CHA	0.73	36	0.23	0.31
OH-11	12.5	0.40	160	4 days	CHA	0.74	40	0.23	/
OH-12	12.5	0.40	160	4 days	CHA	0.83	38	0.20	/
OH-13	12.3	0.45	160	4 days	CHA	0.65	40	0.20	0.32
OH-14	12.6	0.45	160	4 days	CHA	0.61	31	0.13	0.32
OH-15	12.6	0.50	160	4 days	CHA+ Layer[f]	0.66	29	0.16	/
OH-16	13.0	0.51	160	4 days	CHA+ Layer[f]	0.71	35	0.12	/
OH-17	12.2	0.67	160	4 days	Layer[f]	0	N.A	N.A	/

Sample name[a]	H_2O/Si	OSDA-OH^-/Si	Synthesis Temp (°C)	Synth. time	Formed phase	Yield[b]	Si/Al_F[c]	Co/Al_F [c] DCC	$V_{micropore}$ (cm^3/g)
III) H_2O-series: Variation of water concentration : H_2O/Si: [5-101]									
H_2O-1	5	0.35	160	4 days	CHA	0.81	39	0.26	0.31
H_2O-2	7.5	0.35	160	4 days	CHA	/	35	0.31	/
H_2O-3	7.5	0.35	160	4 days	CHA	0.83	39	0.22	0.33
H_2O-4	10	0.35	160	4 days	CHA	0.79	38	0.22	0.33
<IZC-St.>[d]	12.5	0.35	160	4 days	CHA	0.73	36	0.23	0.31
H_2O-5	15	0.35	160	4 days	CHA	0.84	37	0.22	0.32
H_2O-6	18	0.35	160	4 days	CHA	0.77	40	0.22	/
H_2O-7	20	0.35	160	4 days	CHA	0.76	38	0.21	/
H_2O-8	25	0.35	160	4 days	CHA	0.67	31	0.24	/
H_2O-9	30	0.35	160	4 days	CHA	0.79	36	0.20	/
H_2O-10	40	0.35	160	4 days	CHA	0.81	41	0.20	0.31
H_2O-11	50	0.35	160	4 days	CHA	0.84	38	0.17	/
H_2O-12	75	0.35	160	4 days	CHA	0.71	31	0.21	0.31
H_2O-13	101	0.35	160	4 days	CHA	0.74	35	0.14	0.31
H_2O-14	101	0.35	160	4 days	CHA	0.64	39	0.17	/
IV) Time-series: Variation of synthesis duration: t= [2 hours-18 days]									
Time-1	12.5	0.35	160	2 hours	CHA[f]	low	/	/	/
Time-2	12.5	0.35	160	3 hours	CHA	0.57	29	0.32	0.33
Time-3	12.5	0.35	160	3 hours	CHA	0.56	34	0.31	0.31
Time-4	12.5	0.35	160	6 hours	CHA	0.64	35	0.33	/
Time-5	12.5	0.35	160	6 hours	CHA	0.64	34	0.32	0.31
Time-6	12.5	0.35	160	6 hours	CHA	0.50	29	0.30	/
Time-7	12.5	0.35	160	6 hours	CHA	/	30	0.29	/
Time-8	12.5	0.35	160	24 hours	CHA	0.52	37	0.27	/
Time-9	12.5	0.35	160	24 hours	CHA	0.55	33	0.29	/
Time-10	12.5	0.35	160	2 days	CHA	0.65	34	0.27	/
Time-11	12.5	0.35	160	2 days	CHA	0.54	33	0.27	/
<IZC-St.>[d]	12.5	0.35	160	4 days	CHA	0.73	36	0.23	0.31
Time-12	12.5	0.35	160	8 days	CHA	0.82	34	0.20	/
Time-13	12.5	0.35	160	8 days	CHA	0.74	35	0.21	/
Time-14	12.5	0.35	160	12 days	CHA	0.84	34	0.14	/
Time-15	12.5	0.35	160	12 days	CHA	0.81	41	0.18	0.32
Time-16	12.5	0.35	160	16 days	CHA	/	34	0.15	/
Time-17	12.5	0.35	160	18 days	CHA	0.89	60	0.16	0.32

Sample name[a]	H_2O/Si	OSDA-OH^-/Si	Synthesis Temp (°C)	Synth. time	Formed phase	Yield[b]	Si/Al_F[c]	Co/Al_F [c] DCC	$V_{micropore}$ (cm^3/g)
V) Temperature-series: Variation of synthesis temperature: T= [120°C-180°C][e]									
Temp-1	12.5	0.35	100	4 days	CHA	n.d.	32	0.29	0.32
Temp-2	12.5	0.35	100	4 days	CHA	0.59	29	0.32	/
Temp-3	12.5	0.35	120	4 days	CHA	0.70	43	0.33	0.31
Temp-4	12.5	0.35	140	4 days	CHA	0.66	28	0.33	/
Temp-5	12.5	0.35	140	4 days	CHA	0.64	34	0.27	/
<IZC-St.>[d]	12.5	0.35	160	4 days	CHA	0.73	36	0.23	0.31
Temp-6	12.5	0.35	175	4 days	CHA	0.70	32	0.16	/
Temp-7	12.5	0.35	100	24 hours	CHA	low	/	/	/
Temp-8	12.5	0.35	120	24 hours	CHA	0.55	25	0.21	0.32
Temp-9	12.5	0.35	140	24 hours	CHA	0.67	28	0.34	0.34
Temp-10	12.5	0.35	175	24 hours	CHA	0.83	32	0.23	0.34
Temp-11	12.5	0.35	120	6 hours	CHA+FAU	/	/	/	/
Temp-12	12.5	0.35	140	6 hours	CHA	0.49	20	0.07	/
Temp-13	12.5	0.35	140	6 hours	CHA	0.56	24	0.19	/
Temp-14	12.5	0.35	175	6 hours	CHA	0.72	33	0.26	0.32
Temp-15	12.5	0.35	180	12 days	CHA	n.d.	31	0.07	0.29
VI) Constant initial pH-series: OH^-/H_2O = 0.028 (H_2O/Si and OSDA-OH/Si both varying)									
OH/H_2O-1	4.9	0.13	160	4 days	CHA	0.87	47.3	0.09	/
OH/H_2O-2	6.3	0.17	160	4 days	CHA	0.85	46.2	0.11	
IZC-St.3	12.5	0.35	160	4 days	CHA	0.74	39.3	0.23	0.31
OH/H_2O-4	24.8	0.70	160	4 days	CHA	0.48	25.4	0.12	
VII) MFI-to-CHA: Variation in synthetic source (CBV8014, ZSM-5)									
MFI-1	12.5	0.35	160	19 hours	CHA	0.63	26.2	0.06	

[a] All syntheses originate from synthesis batch compositions: ~**1**SiO2:**40**Al^{-1}:**x**$TMAda^+$:**x**OH^-:**y** H_2O with CBV780 as Si and Al source; [b] Yield = [dry product weight (g)*(1-0.2 wt. fraction OSDA)] / [initial g(SiO_2+AlO_2)$_{dry}$]; [c] From ICP-AES; [d] <IZC-St.> are average values of standard zeolite condition samples; [e] Results of 6 and 24 hours synthesis condition at 160°C can be found in the IV) time series: Time-4, Time-5, Time-6 and Time-7 for 6 hours synthesis and Time-8, Time-9 for 24 hours synthesis. [f] Low crystallinity for the CHA phase in the mixture.

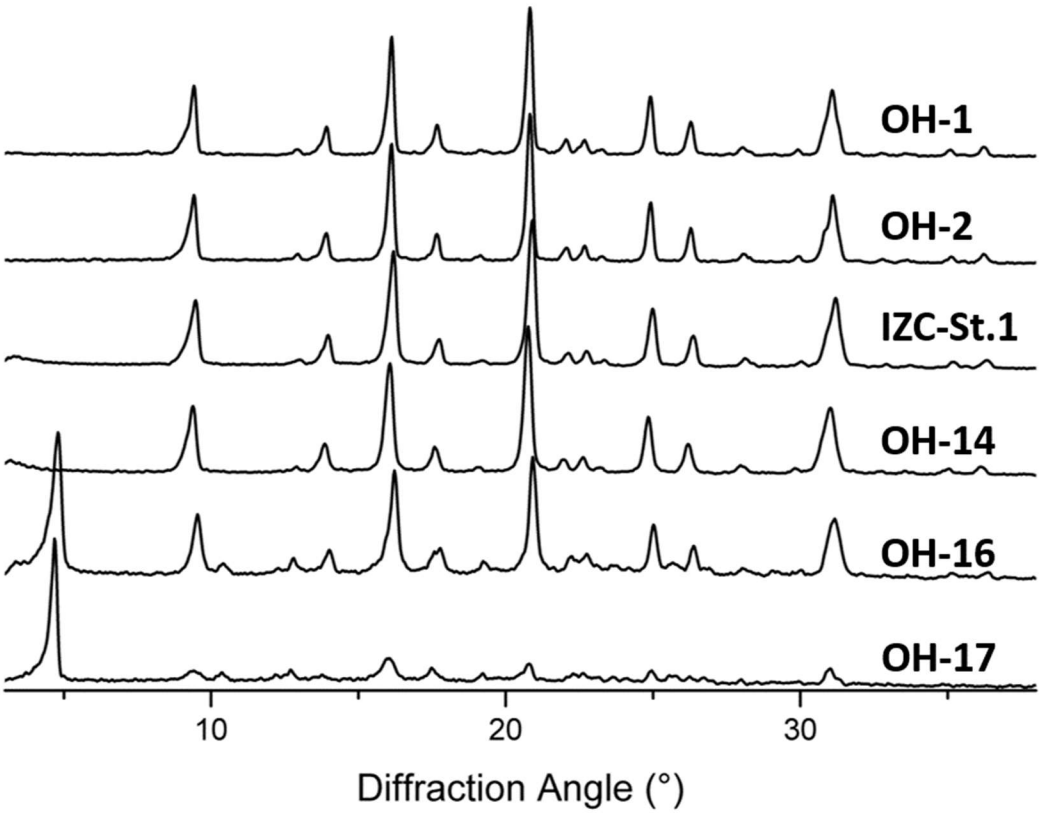

Figure S12. Normalized powder XRD patterns of as-synthesized products made with different TMAdaOH content.

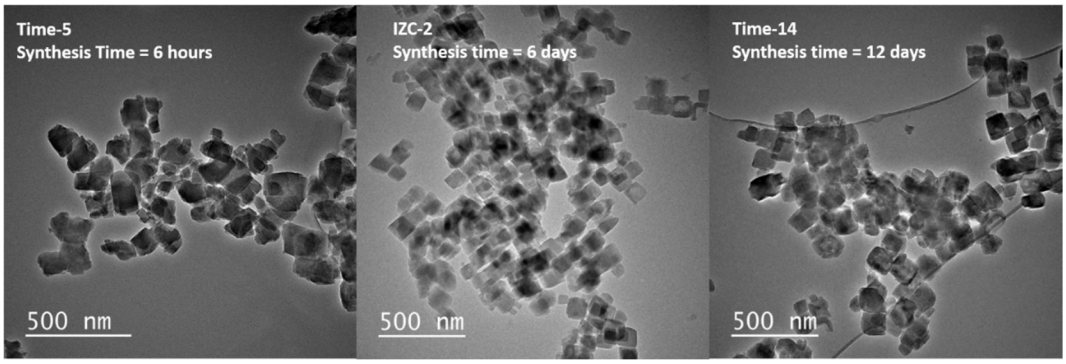

Figure S13. TEM images of representative SSZ-13 particles made from standard batch composition (**1**SiO_2: **0.025**Al: **0.35** $TMAda^+$:**0.35** OH^-:**12.5** H_2O) with variable synthesis times. Typical crystals are 100-200nm in cross-length with an irregular to cubic shape.

S.4.1 . Deconvolution of synthesis parameter effects on DCC.

A series of experiments have been set-up with similar initial pH (OH^-/H_2O is fixed at 0.028) by both varying OSDA content (TMAdaOH/Si) and dilution (H_2O/Si). Exact compositions are presented in Table S4 (series VI). In figure S14-A, one can compare the resulting DCC values of this series (with changing H_2O/Si) with the results of the TMAdaOH series (Figure 1A, Table S4-Series II). Seemingly, the DCC values are in accordance with the TMAda-OH/Si concentration trend with constant H_2O content (H_2O/Si=12.5, Table S4, series II). In figure S14-B, one can see that these samples have much less of a similar relation when compared to the variable dilution series (Table S4 (series III)) keeping in mind that the OSDA/Si is changing as well. The interactions between the mineralizing agent (OH^-) with Si (and Al sources) are likely more important to the outcome in terms (of kinetics and) DCC, rather than merely the overall contribution of hydroxide concentration (OH/Si, linked to pH). Likewise, such parameters (OSDA/Si) are also more important for zeolite crystallization in general than the effect of pH on its own.[4]

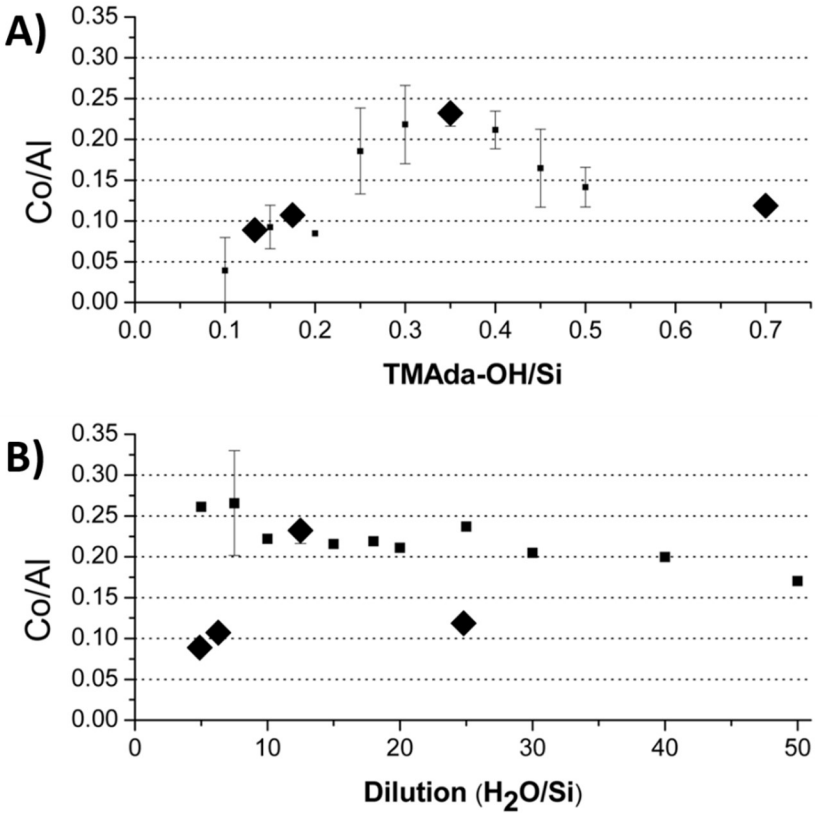

Figure S14. Effect of TMAda-OH and H_2O/Si on DCC (Co/Al) of the resulting SSZ-13 materials in syntheses with equal starting pH of the liquid (OH^-/H_2O=0.028). All zeolites are made with US-Y Si/Al 40 (CBV780), water and aqueous TMAdaOH as starting reagents under stable conditions: 160°C, 4 days and 600 rpm. Full diamonds refer to DCC outcomes of SSZ-13 recipes with constant OH^- but against variable TMAdaOH (A) and dilution (B) respectively. The reader is referred to table S4-Series VI for exact batch compositions.: **1**SiO_2: **0.025**Al: **x**$TMAda^+$: **x**OH^-: **y**H_2O (diamonds). The full squares (with error bars) refer to data from TMAdaOH variations (A) and dilution (B) respectively, as in Figure 1 in the main text.

S4.2. Influence of solid yield on DCC.

Figure S15 demonstrates that the synthesis yield of standard recipes (**1**SiO2: **0.025** Al:**0.35** $TMAda^+$:**0.35** OH^-:**12.5** H_2O; 160°C) gradually increases with time from 57% (3h) to 89% (18d). In the meantime DCC values (in Co/Al) drop from 0.31 at 3h to 0.15 (16 days). The initial crystalline solid fraction at 3 hours synthesis (solid yield <0.56>, nearly 100% crystallinity as compared to the most crystalline sample in the time series) has a very high DCC (Co/Al=0.33). The significantly lower DCC values (~50% lower) at very long synthesis times are remarkable. Given the dynamic and coupled dissolution and precipitation equilibria taking place during synthesis, it could be that later formed SSZ-13 have other DCC values. Nevertheless, simple calculations demonstrate that the additionally created solid yield cannot explain the overall DCC drop, even considering assembly of later formed SSZ-13 with Co/Al=0. This theory is supported by using DCC and yield data in the paragraph underneath.

Example: DCC evolution from 4 days to 12 days (using average values).

At four days, 0.73 gram yield SSZ-13 is obtained from each gram of source FAU (solid yield) with Co/Al=0.23. Considering Si/Al remains constant in materials from 4 days and 12 days synthesis (Si/Al= 36 vs.37.5 respectively) an additional growth of solid materials to 0.825 $g_{SSZ\text{-}13}/g_{FAU}$ with Co/Al=0 for the newly formed fraction would still result in an overall composition of Co/Al=0.204 instead of the observed average Co/Al= 0.162. Hereby proving that DCC alterations do depend on more than differences in additional growth assembly alone. The temperature series (175 and 180°C) also confirmed very low DCCs by prolonged exposures.

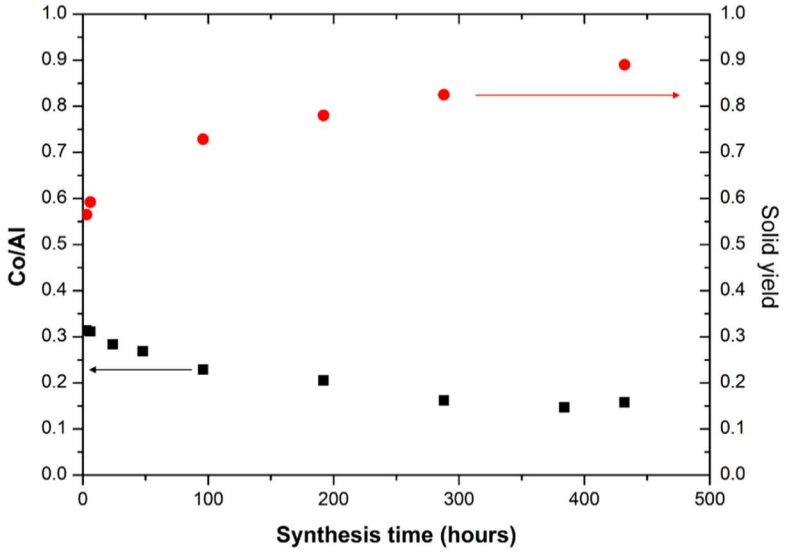

Figure S15. Evolution of synthesis yield and DCC during prolonged maturation of SSZ-13 synthesis media. Some data points for solid yield are missing due to lack of accurate data.

Section S5. Methane partial oxidation (MPO) on Fe-SSZ-13 from different recipes.

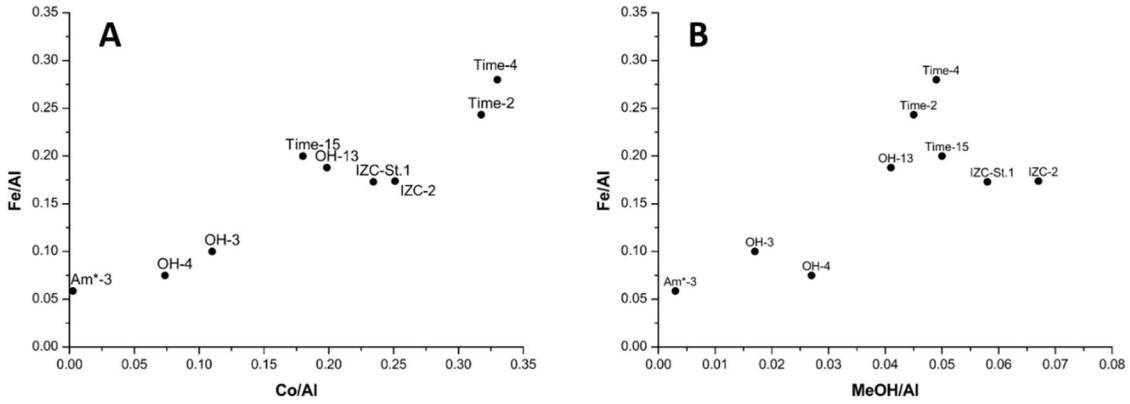

Figure S16. Fe uptake (normalized per Al) vs DCC and vs Methane partial oxidation (MPO) productivity on variably synthesized SSZ-13. Each synthesis label refers to sample names in Table S1 and Table S4. A) Fe-uptake (Fe/Al) versus DCC, so effectively Fe- vs Co-uptake of tailored SSZ-13. B) Fe-uptake versus MeOH productivity tailored SSZ-13. Each dot represents one SSZ-13 synthesis and their labels can be traced in the supporting information (Table S1, Table S4). Compare Fig. S16B to Fig. 3.

Section S6. Temporal analysis of FAU-to-CHA synthesis

Table S5 and Figures S17-S20 contain characterization data of the intermediate phases gathered from temporal analysis of FAU-to-CHA conversion. All these entries are individually run identical synthesis (to avoid perturbation in sampling). Section S6.1. contains additional synthesis tests (Table S6) using intermediate isolated phases, to explore or clarify the role of the intermediate phases on DCC.

➔ **Table S5.** Chemical composition and yield of products produced during high Si FAU-to-CHA conversion.

Synthesis time (hours)	Solid phase[a]							Liquid phase[b]		
	CHA% [c]	dry yield[d]	Si/Al	Al yield	Si yield	TGA fr.[e] [150-300°C]	TGA fr.[e] [300-800°C]	Si/Al	Al yield	Si yield
0	0	1	40	1	1	/	/	/	0	0
0.25	0	0.50	23	0.83	0.49	0.21	0.12	121	0.17	0.51
0.33 (A)	0	0.22	13	0.51	0.21	0.14	0.09	94	0.31	0.71
0.33 (B)	0	0.05	4	0.53	0.04	/	/	73	0.53	0.96
0.5	0	0.04	3	0.44	0.03	0.05	0.05	64	0.62	0.97
0.75	0	0.04	3	0.43	0.03	0.06	0.05	80	0.49	0.97
1	0	0.04	3	0.46	0.03	0.04	0.05	73	0.54	0.97
1.25	5	0.06	4	0.49	0.05	0.15	0.09	69	0.56	0.95
1.5	9	0.11	5	0.51	0.09	0.06	0.09	75	0.49	0.90
1.60	22	0.36	20	0.73	0.35	0.27	0.13	147	0.18	0.65
1.75	29	0.17	9	0.70	0.16	0.10	0.12	120	0.29	0.84
2	53	0.25	14	0.72	0.24	0.11	0.16	206	0.15	0.76
2.5	93	0.50	21	0.97	0.49	0.02	0.23	471	0.04	0.51
3	100	0.55	22	1.01	0.53	0.02	0.23	1153	0.02	0.46

[a] Solid residue after centrifugal separation. [b] Supernatant after centrifugal separation. ICP-based data for the supernatant (Si/Al) are obtained by drying-out the liquid phase. Liquid Al and Si yields are based on Si/Al of the liquid and the dry solid yields.[c] Relative **CHA**-crystallinity calculated as the sum of selected SSZ-13 peaks (at 9.5°, 16.2° and 20.9°, as-synthesized material), compared to sum of the selected SSZ-13 peaks of a reference sample fixed at 100% crystallinity. The 3 hour sample is used as reference (high intensity) and has typical SSZ-13 properties (TGA, physisorption, …). [d] Dry yield = solid yield based on weighing + a correction based on TGA (dry TO_2 remaining weight after TGA to 800°C) versus the input TO_2 weight. [e] Fraction of weight lost between certain temperatures, from TGA (e.g. Figure S19).

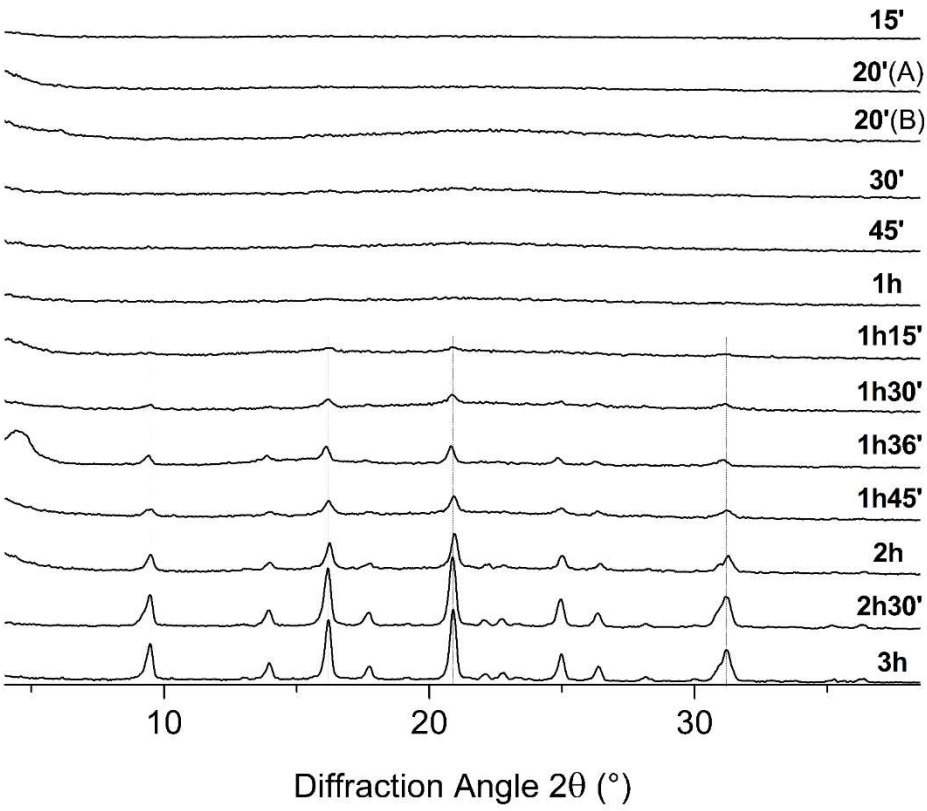

Figure S17. Stacked powder XRD patterns (10min beam time) of solids obtained after short hydrothermal synthesis [15 min. to 3 hours] under standard conditions (**1**SiO_2: **0.025**Al: **0.35**$TMAda^+$: **0.35**OH^-: **12.5**H_2O, 600 rpm, 160 °C).

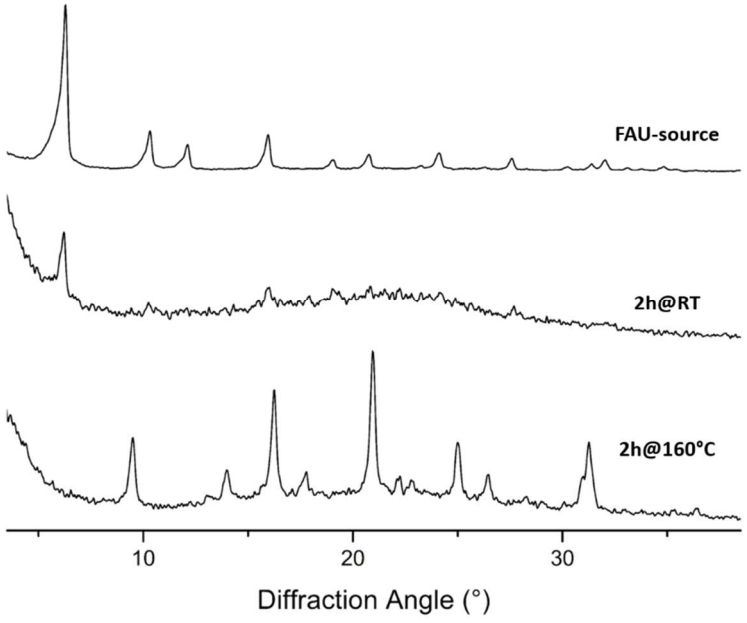

Figure S18. Normalized powder XRD patterns of the starting sources (CBV780; FAU), the solid products after 2 hours of room temperature aging and after 2 hours of hydrothermal synthesis under standard conditions (1SiO_2: 0.025Al: 0.35$TMAda^+$: 0.35OH^-: 12.5H_2O, 600 rpm, 160 °C).

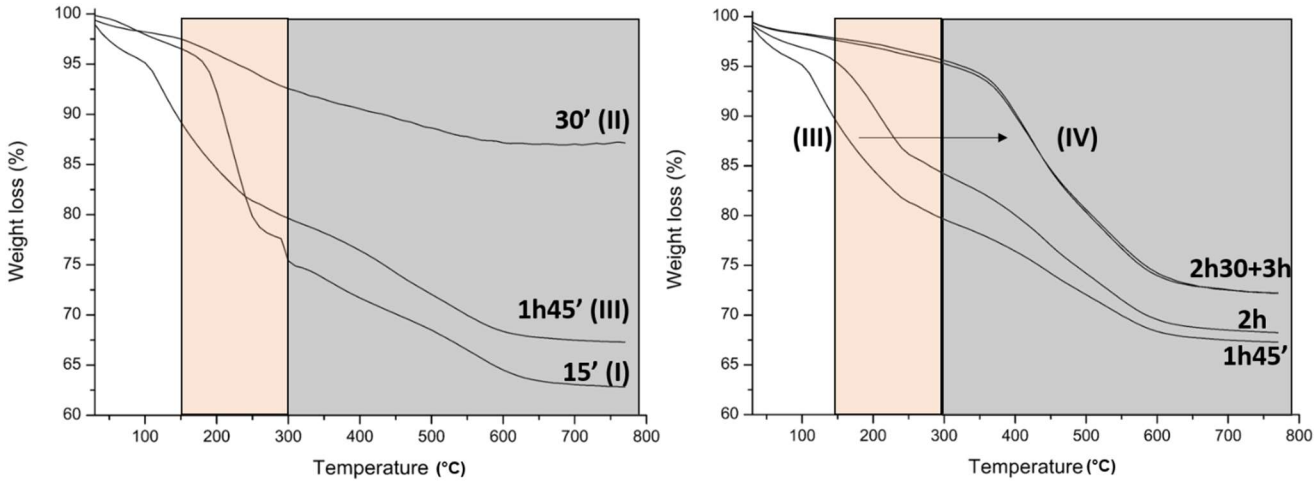

Figure S19. Representative TGA profiles for each synthesis stage (Stage I-IV). The measured samples are solid fractions separated after variable oven times. The salmon pink fraction represents weight loss fractions between 150°C and 300°C. The grey fraction represents weight loss fractions between 300°C and 800°C. Quantified weight loss fractions are listed in Table S5.

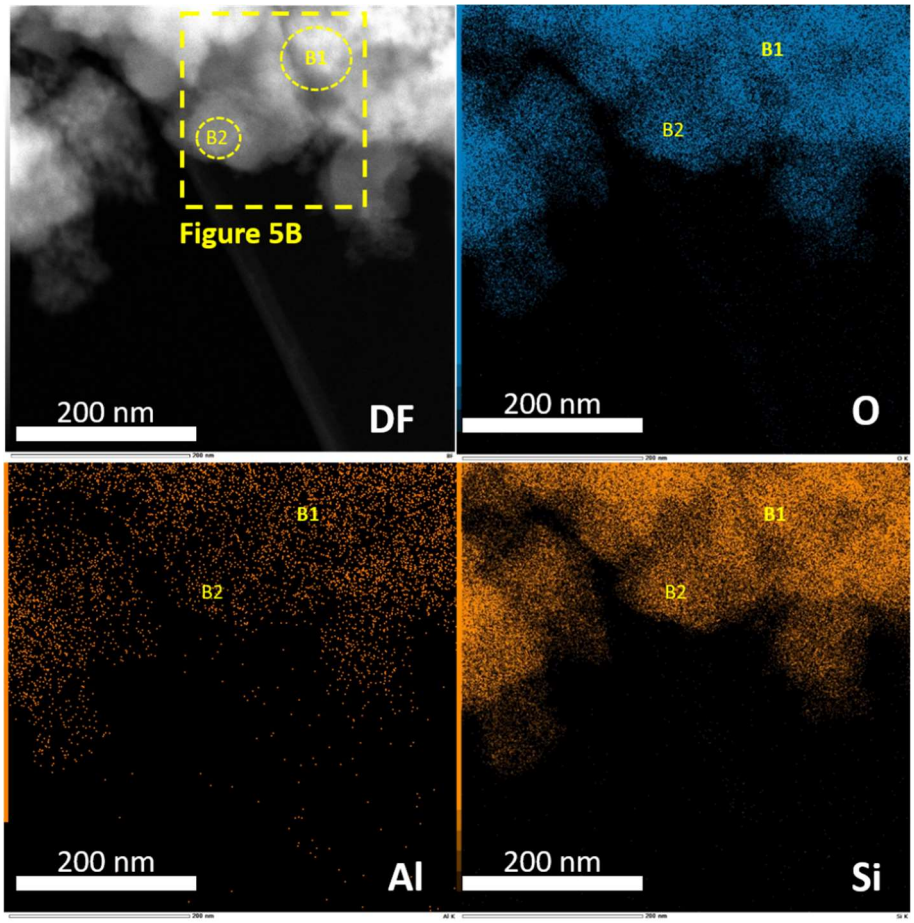

Figure S20. STEM-EDX image of the selected TEM region in Figure 5B (circles here in Fig. S20 approximately). Up-left is given a dark field (DF) image of the selected region. Underneath (bottom-left), the elemental mapping of Al is demonstrated. Up-right and bottom-right, contains elemental mappings of O and Si respectively. Seemingly, all elements are homogeneously distributed within the selected aggregate. No significant difference in Si or Al distributions between the crystalline regions (B2, from FFT) and the surrounding amorphous regions is observed.

S6.1. DCC potential of the solid phase and liquid supernatant present at induction

For these tests a standard IZC synthesis (1**SiO_2:** 0.025**Al:** 0.35**TMada$^+$:** 0.35**OH^-:** 12.5 **H_2O**) is stopped during the induction process after 1hour, the solid and liquid phase are separated according to procedures described earlier (2.3., Experimental Section) and both fractions (solid and the liquid supernatant) are immediately used as respectively the Al and Si source in this cross test. Colloïdal silica (LUDOX HS-40, Sigma Aldrich) is added as Si-source to the Al rich solids and $Al(OH)_3$ (Sigma Aldrich) is added to the Si-rich supernatant solution to attain an overall composition: 1**SiO_2:**0.025**Al:**0.35**TMada$^+$:**0.35**OH^-:**18.5**H_2O**. These compositions are also made using the typical ingredients of IZC synthesis and amorphous syntheses for comparison (using CBV780 and LUDOX-HS40+$Al(OH)_3$ respectively). All experiments -having different sources but similar composition- are made using typical conditions (160°C, 600 rpm internal stirring) and according to the procedures described in Section 2.3. The results of those cross tests are summarized in table S6. All four syntheses yield fully crystalline SSZ-13 after 24 hours of synthesis, have comparable Si/Al and show high DCC capacity for SSZ-13 using sources that originate from FAU. Both solid and liquid fractions present during induction (of course subject to the separation used in our method) are capable to form SSZ-13 with high DCC, hereby seemingly confirming a crucial role for both liquid and solid phases derived from FAU towards SSZ-13 with high DCC.

Table S6. Characterisation of the solid products of SSZ-13 synthesis using different sources under identical compositions **1**SiO_2: **0.025**Al: **0.35**TMAda$^+$: **0.35**OH^-: **18.5** H_2O. The resulting SSZ-13 materials have different DCC outcome.

Al source	Si-source	Synthesis time	Si/Al[a]	Co/Al[a] (DCC)
US-Y (Si/Al=40)	US-Y (Si/Al=40)	24 hours	26	0.28
Solid phase	LUDOX HS-40 (+solid phase)	24 hours	25	0.33
$Al(OH)_3$ + liquid supernatant	liquid supernatant (Si/Al ≥ 75)	24 hours	23	0.28
$Al(OH)_3$	LUDOX HS-40	24 hours	22	0.04

[a]Si/Al_S and DCC molar ratios of the solid calcined zeolite fraction as determined by ICP-AES.

Section S7. References.

1. Bols, M. L.; Hallaert, S. D.; Snyder, B. E. R.; Devos, J.; Plessers, D.; Rhoda, H. M.; Dusselier, M.; Schoonheydt, R. A.; Pierloot, K.; Solomon, E. I.; Sels, B. F., Spectroscopic Identification of the α-Fe/α-O Active Site in Fe-CHA Zeolite for the Low-Temperature Activation of the Methane C–H Bond. *Journal of the American Chemical Society* **2018,** *140* (38), 12021-12032.
2. Dědeček, J.; Sobalík, Z.; Wichterlová, B., Siting and Distribution of Framework Aluminium Atoms in Silicon-Rich Zeolites and Impact on Catalysis. *Catalysis Reviews* **2012,** *54* (2), 135-223.
3. Mlekodaj, K.; Dedecek, J.; Pashkova, V.; Tabor, E.; Klein, P.; Urbanova, M.; Karcz, R.; Sazama, P.; Whittleton, S. R.; Thomas, H. M.; Fishchuk, A. V.; Sklenak, S., Al Organization in the SSZ-13 Zeolite. Al Distribution and Extraframework Sites of Divalent Cations. *The Journal of Physical Chemistry C* **2018**.
4. Burton, A. W.; Zones, S. I., Chapter 5 Organic molecules in zeolite synthesis: Their preparation and structure-directing effects. In *Studies in Surface Science and Catalysis*, Jiří Čejka, H. v. B. A. C.; Ferdi, S., Eds. Elsevier: 2007; Vol. Volume 168, pp 137-179.